Studying the proton rms radii of Li and B isotopes through elastic scattering*

Ling-Hao Wang (汪凌昊)[1,2†] Fang-Fang Duan (段芳芳)[1] Kang Wang (王康)[1,2] Guo Yang (杨过)[1,2]
Xing-quan Liu (刘星泉)[3] Yan-Yun Yang (杨彦云)[1,2]

[1]CAS Key Laboratory of High Precision Nuclear Spectroscopy, Institute of Modern Physics, Chinese Academy of Sciences, Lanzhou 730000, China
[2]School of Nuclear Science and Technology, University of Chinese Academy of Sciences, Beijing 100080, China
[3]Institute of Nuclear Science and Technology, Sichuan University, Sichuan, 610000, China

Abstract: The root mean square (rms) nuclear proton radii of ^{6,7,8}Li and ^{10,11}B projectiles are systematically investigated by analyzing elastic scattering data from target nuclei with mass numbers ranging from 40 to 209 at incident energies exceeding Coulomb barriers. The analyses employ a consistent single-folding model potential based on the Bruyères Jeukenne-Lejeune-Mahaux (JLMB) nucleon-nucleus interaction model, incorporating 112 sets of elastic scattering data to derive the projectile nuclear radii. This approach yields individual radii for each set, from which the mean rms proton radius is extracted as a characteristic parameter for the projectile nuclei. The rms proton radii of ^{6,7}Li and ^{10,11}B nuclei, obtained from optical model fits, demonstrate good agreement with experimental measurements and existing theoretical predictions. Notably, a significantly smaller nuclear radius of ^{8}Li is observed compared to values derived from intermediate-energy proton elastic scattering cross-section measurements, which may be attributed to additional dynamical effects specific to the ^{8}Li projectile.

Keywords: RMS radii, optical model potentials, elastic scattering

DOI: 10.1088/1674-1137/ae1183 **CSTR:** 32044.14.ChinesePhysicsC.50024105

I. INTRODUCTION

The nuclear radii correspond to a pivotal observable parameter for elucidating nuclear structure [1]. By definition, the charge distribution of a nucleus is characterized by $\langle r^2\rangle_{ch}$, whereas the neutron and proton distributions are described by $\langle r^2\rangle_n$ and $\langle r^2\rangle_p$, respectively.

Experimentally, several techniques have been used to determine the root mean square (rms) nuclear charge radii. Three methods have proven particularly effective: electron scattering experiments, muonic spectra analyses, and measurements of optical and K_α X-ray isotope shifts [2]. For example, electron scattering experiments with energies up to 125 and 150 MeV have been conducted [3]. These experiments measured the angular distribution of cross sections related to form factors. This measurement, in turn, enables the deduction of the nuclear charge distribution.

Muonic spectra offer an alternative approach to determine $\langle r^2\rangle_{ch}$. Muons are 207 times heavier than electrons. Given this greater mass, they have smaller orbital radii and a higher degree of overlap with the nuclear wave function. Spectra from the $2p\to 1s$ muon de-excitation process have been used to extract $\langle r^2\rangle_{ch}$ [4]. Additionally, isotope shifts cause differences in atomic spectra. When these spectral differences are combined with precise atomic structure calculations, they can also yield the rms nuclear charge radius [5].

The rms nuclear matter radii can be determined by analyzing the interaction cross sections in heavy ion collisions at high energies. Classically, the interaction cross section σ can be expressed as $\sigma=\pi(R_T+R_P)^2$, with R_T and R_P denoting the radii of the target and projectile nuclei, respectively [6−8], and quantization analysis is accomplished through the Glauber model [9−11]. Using peripheral collisions, the rms radii of point proton distributions can be obtained via charge-changing interaction cross sections at intermediate energies given that these cross sections are related to both proton and neutron distributions [12, 13]. Moreover, the rms radii of point proton distributions can be derived from charge radii data using the relation [14]: $\sqrt{\langle r^2\rangle_p}=\sqrt{\langle r^2\rangle_{ch}-0.76+0.11(N/Z)}$.

Theoretically, advanced approaches, such as ab initio theory [15, 16], shell model theory [17], and mean field theory [18−20] are extensively used to calculate the rms nuclear charge, neutron, and proton radii.

Optical Model Potentials (OMPs) play a critical role in understanding nuclear reaction mechanisms. OMPs are

Received 18 August 2025; Accepted 10 October 2025; Accepted manuscript online 11 October 2025

* This work was supported by the National Key R&D Program of China (2023YFA1606702) and the Natural Science Foundation for Young Scientists of Gansu Province, China (24JRRA035).

† E-mail: wanglinghao@impcas.ac.cn

obtained by fitting experimental data. Systematic OMPs are derived from a broad range of target nuclei and projectile energies [21−23]. They significantly decrease uncertainties and enhance reliability of predictions [21]. Xu *et al*. conducted sensitivity tests of potential parameters in 2013 [23], while Zhang *et al*. reported on the sensitivity of neutron density distributions for OMPs in 2014 [24]. In 2023, Yang *et al*. applied systematic OMPs to heavy ions [21]. These studies enable the extraction of rms nuclear proton radii with optical model analyses of elastic scattering data. With respect to the isotopes under investigations, elastic electron scattering measurements for ^{6}Li and ^{7}Li and ^{10}B and ^{11}B were reported by F. A. Bumiller in 1972 [25] and T. Stovall in 1966 [26], respectively. However, ^{8}Li is unstable with a half-life of 837.7 ms [27], thereby rendering elastic electron scattering unsuitable to measure its charge radius. Conversely, the use of stable Lithium isotopes (^{6}Li or ^{7}Li) as references via isotope shift measurements determine the charge radius of ^{8}Li [28]. In 2019, Bernhard Maass achieved the first isotope shift measurements for ^{10}B and ^{11}B, and the results indicated an improvement in experimental precision when compared to that of elastic electron scattering [29]. Currently, only the rms radius of the point proton distribution for ^{11}B has been analyzed from charge-changing interactions, as reported by Yoshiko in 2015 [15]. This manuscript is structured as follows. Section II details the formalism considered in the present study, encompassing nucleus-nucleus potential used to extract the rms nuclear proton radii. Section III presents descriptions of angular distributions of elastic scattering with different nucleon density distributions. Section IV discusses results of proton radii and comparisons with other experimental and theoretical results. Finally, in Sec. V, a summary of this study is presented.

II. THEORETICAL CONSIDERATIONS

The angular distributions of elastic scattering were analyzed within the framework of the optical model. The effective interactions are characterized by a long-range repulsive Coulomb potential $V_C(R)$ and a short-range attractive nuclear potential $U_N(R)$, which can be combined as follows:

$$U(R,E_{\rm lab}) = U_N(R,E_{\rm lab}) + V_C(R), \tag{1}$$

Here, $\boldsymbol{R}$ denotes the vector connecting the center of mass (c.m.) of the target nucleus to that of the projectile, while $E_{\rm lab}$ represents incident energy in the laboratory frame. It should be noted that $U_N(R,E_{\rm lab})$ is derived from the Bruyères Jeukenne-Lejeune-Mahaux (JLMB) effective interaction. Thus, it represents an optical potential as opposed to a bare potential. For the Coulomb component $V_C(R)$, we adopted a conventional model. This model assumes a uniform charge distribution in spherical nuclei, and it can be defined as follows:

$$V_C(R) = \begin{cases} \dfrac{Z_P Z_T e^2}{R} & (R > R_C) \\ \dfrac{Z_P Z_T e^2}{2R_c}\left[3 - \dfrac{R^2}{R_C^2}\right] & (R \leqslant R_C) \end{cases}, \tag{2}$$

In this equation, the charge radius R_C was assumed to be $1.3\times(A_P^{1/3}+A_T^{1/3})$ fm, with A_P and A_T denoting the mass numbers of the projectile and target nuclei, respectively. For the nuclear component, the systematic nucleus-nucleus potential proposed in Ref. [21] was employed. The real and imaginary parts of the complex $U_N(R,E_{\rm lab})$ potential were computed using the single-folding model. Renormalization factors N_r and N_i were determined by analyzing experimental data for stable nuclei [21]:

$$U_N(R,E_{\rm lab}) = N_r {\rm Re}[U_{\rm sf}] + N_i {\rm Im}[U_{\rm sf}], \tag{3}$$

Here, $U_{\rm sf}$ denotes the single-folding model potential experienced by a projectile nucleus during its collision with a target nucleus at an incident energy $E_{\rm lab}$. This potential requires renormalization due to the composite nature of the projectile nucleus and can be expressed as follows:

$$U_{\rm sf}(R,E_{\rm lab}) = \sum_{i=p,n}\int \rho_i(\boldsymbol{r}) v(E_{\rm lab}/A_P, |\boldsymbol{s}|){\rm d}\boldsymbol{r}. \tag{4}$$

In this expression, $\boldsymbol{s}=\boldsymbol{R}+\boldsymbol{r}$ denotes the vector from the c.m. of the target to the nucleon of the projectile. The interaction $v(E_{\rm lab}/A_P,|\boldsymbol{s}|)$ between a free nucleon and the target nucleus was assumed to follow the semimicroscopic Lane-consistent JLMB model potential in the present calculations. Additionally, $\rho_i(\boldsymbol{r})$ denotes the nucleon density distribution ($i=p$ for proton and $i=n$ for neutron) within the projectile at position $\boldsymbol{r}$ relative to the c.m. of the projectile. In this study, the proton and neutron density distributions of projectile and target nuclei were obtained from Hartree-Fock calculations based on the SkX parametrization [30].This parameter set is used to explain binding energy differences of mirror nuclei [30], interaction cross section [31], transfer reactions [32], and nuclear charge density distributions [33]. The calculated proton rms radii for ^{6}Li, ^{7}Li, ^{8}Li, ^{10}B and ^{11}B, are 2.104, 2.092, 2.090, 2.325, and 2.303 fm, respectively. By contrast, the corresponding experimental values are 2.46 ± 0.04, 2.315 ± 0.044, 2.212 ± 0.047, 2.29 ± 0.05, and 2.272 ± 0.031 fm [2]. This disparity highlights a significant discrepancy between theoretical predictions and experimental data, especially for lithium isotopes. In particular, single-folding model calculations with smaller rms proton radii yield predicted angular distributions that are shifted toward larger angles when compared to those obtained using the experimental values. This observation suggests that by optimizing the fit between experimental data and theoretical cross sections through adjustments in the nucleon density distributions, the rms proton radii of nuclei can be extracted with increased accuracy.

III. OPTICAL MODEL ANALYSIS

The elastic scattering experimental data for ^{6,7,8}Li and ^{10,11}B projectiles utilized in this study were collected from the EXFOR [34] nuclear reaction database. The data involved target nuclei with mass numbers ranging from 40 to 209 and incident energies exceeding the Coulomb barriers. With these data, the rms proton radii were extracted thrugh optical model analysis based on an updated systematic nucleus-nucleus potential (USNP). This potential demonstrated success in reproducing elastic scattering and total reaction cross-section data for projectiles with mass numbers up to $A\sim 40$, including stable and radioactive nuclei, for incident energies from the vicinity of the Coulomb barrier to approximately 100 MeV/nucleon [21]. In the analysis procedure, each set of angular distribution data was individually fitted by altering the nucleon density distributions. The standard minimum χ^2 was employed to achieve an optimal description of the experimental data. Mathematically, χ^2 can be defined as

$$\chi^2=\frac{1}{N}\sum_{i=1}^{N}\left[\frac{\sigma_i^{\rm th}(\theta_i)-\sigma_i^{\rm exp}(\theta_i)}{\Delta\sigma_i^{\rm exp}(\theta_i)}\right]^2. \quad (5)$$

where N denotes the total number of data points in each angular distribution dataset, $\sigma_i^{\rm th}$ denotes the theoretical cross section at scattering angle θ_i, and $\sigma_i^{\rm exp}$ and $\Delta\sigma_i^{\rm exp}$ denote the corresponding experimental cross section and its associated uncertainty, respectively. In particular, $\sigma_i^{\rm th}$ was calculated using the USNP with various projectile density distributions. These distributions were generated by rescaling the original Hartree-Fock densities, where the rms radii of the resulting nucleon density distributions were varied by a factor α in the range of 0.60−1.40 with a step size of 0.01. The rescaling process was accomplished by replacing the original density distribution $\rho(r)$ with $\rho(r/\alpha)/\alpha^3$. A brief justification of this method is provided. Density distribution $\rho(r)$ follows a simple conservation law:

$$\int\rho(r)\mathrm{d}\tau=\int\rho(r)r^2\mathrm{d}r=\text{constant},$$

We replace $\rho(r)$ with $\rho(r/\alpha)$ and add a factor λ to maintain conservation:

$$\int\rho(r)r^2\mathrm{d}r=\lambda\int\rho\left(\frac{r}{\alpha}\right)r^2\mathrm{d}r=\text{constant},$$

Change variables as $t=\dfrac{r}{\alpha}$:

$$\int\rho(r)r^2\mathrm{d}r=\lambda\alpha^3\int\rho(t)t^2\mathrm{d}t=\text{constant},$$

This leads to the following expression:

$$\lambda=\alpha^3.$$

The rescaled density distribution is $\rho(r/\alpha)/\alpha^3$. Subsequently, we obtain the relationship between rms radii, and the rms radii can be defined as follows:

$$\langle r^2\rangle=\frac{\int\rho(r)r^2\mathrm{d}\tau}{\int\rho(r)\mathrm{d}\tau},$$

Rescaling the density distribution alters the rms radii:

$$\langle r'^2\rangle=\frac{\frac{1}{\alpha^3}\int\rho(r/\alpha)r^2\mathrm{d}\tau}{\frac{1}{\alpha^3}\int\rho(r/\alpha)\mathrm{d}\tau},$$

Implement $\langle r^2\rangle/\langle r'^2\rangle$ and change variables as $t=\dfrac{r}{\alpha}$:

$$\langle r^2\rangle/\langle r'^2\rangle=\frac{\int\rho(r)r^4\mathrm{d}r}{\alpha^2\int\rho(t)t^4\mathrm{d}t}=\frac{1}{\alpha^2}.$$

After rescaling the density distribution, rms radii are represented as

$$\langle r'^2\rangle=\alpha^2\langle r^2\rangle.$$

Subsequently, the newly created density distribution for each dataset was input into the SFRESCO computer code to compute the differential cross sections and determine optimal value of the rms radii. To obtain more accurate rms proton radii for the nuclei under investigation, the experimental data were extensively compared with the results of optical model calculations with modified nucleon density distributions. The findings are presented in Figs. 1, 2, and 3 for ^{6}Li elastic scattering from medium - mass and heavy targets, in Figs. 4 and 5 for ^{7}Li, in Fig. 6 for ^{8}Li, and in Fig. 7 for ^{10}B and ^{11}B. The blue dashed curves denote optical model calculation results using the searched nucleon density distributions, without any adjustments to the optical model parameters of the USNP. The overall agreement between the experimental data and the fitted angular distributions is quite satisfactory, as fur-

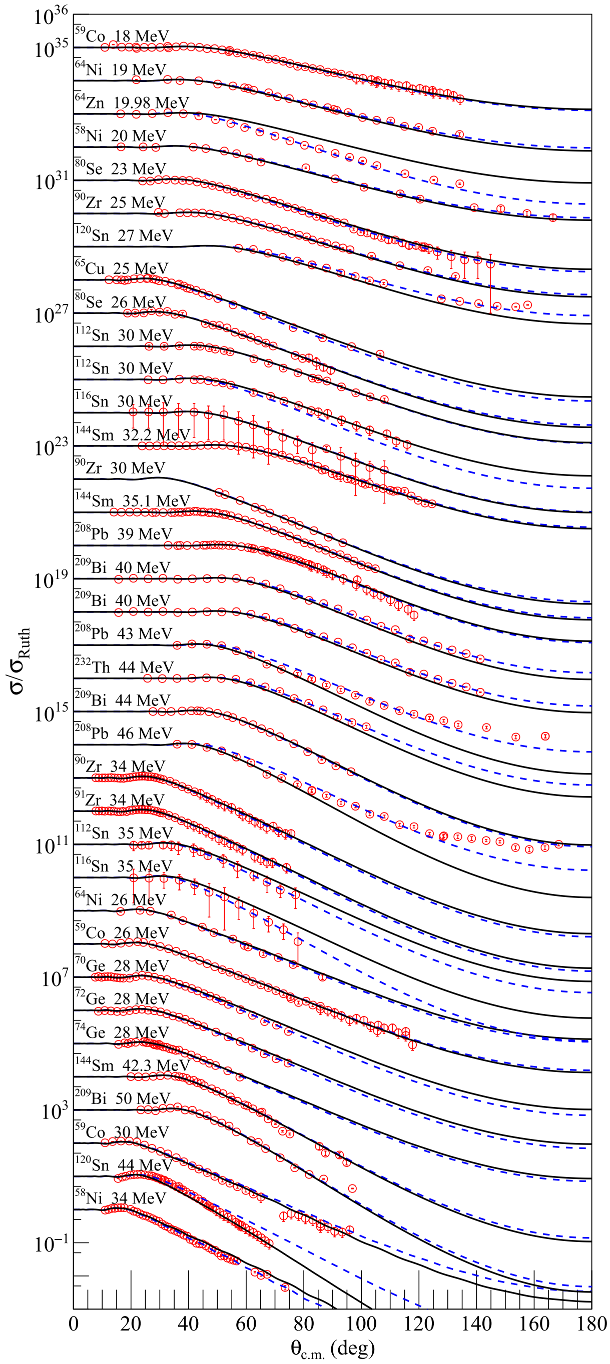

Fig. 1. (color online) Comparisons between optical model calculations and experimental data for ^{6}Li elastic scattering from medium mass and heavy targets at incident energies indicated in the figure. The blue dashed and black solid curves denote results calculated with optimal and average values of rms proton radii, respectively. The datasets are offset for optimum view. The experimental data are from Refs. [35−54].

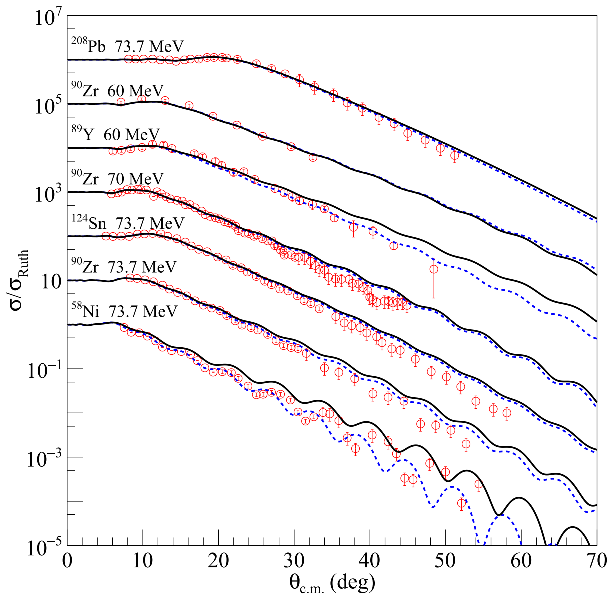

Fig. 2. (color online) Same as Fig. 1 albeit for ^{6}Li at higher energies. The experimental data are from Refs. [55−57].

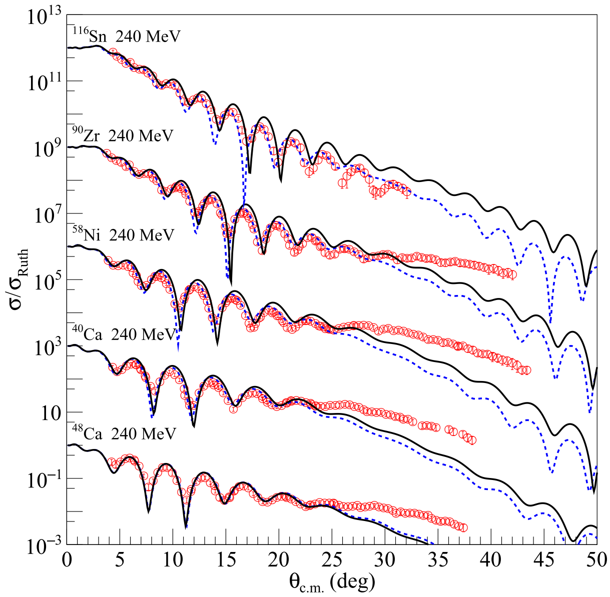

Fig. 3. (color online) Same as Fig. 1 albeit for ^{6}Li at higher energies. The experimental data are from Refs. [58−60].

ther corroborated by the χ^2 values tabulated in Table 1. When compared with the calculations using the original nucleon distributions, significant improvements were noted in describing elastic cross sections.

This outcome indicates that nucleon density distributions deviating from those predicted by Hartree-Fock calculations are necessary to more accurately reproduce the elastic scattering data. It is important to note that several factors, including experimental uncertainties, channel coupling effects, and values of target nuclei radii, affect the angular distributions of elastic scattering, thereby impacting the precision of the extracted projectile rms proton radii. Nevertheless, systematic analysis incorporating a comprehensive set of experimental data is expected to yield relatively reliable rms proton radius values. As

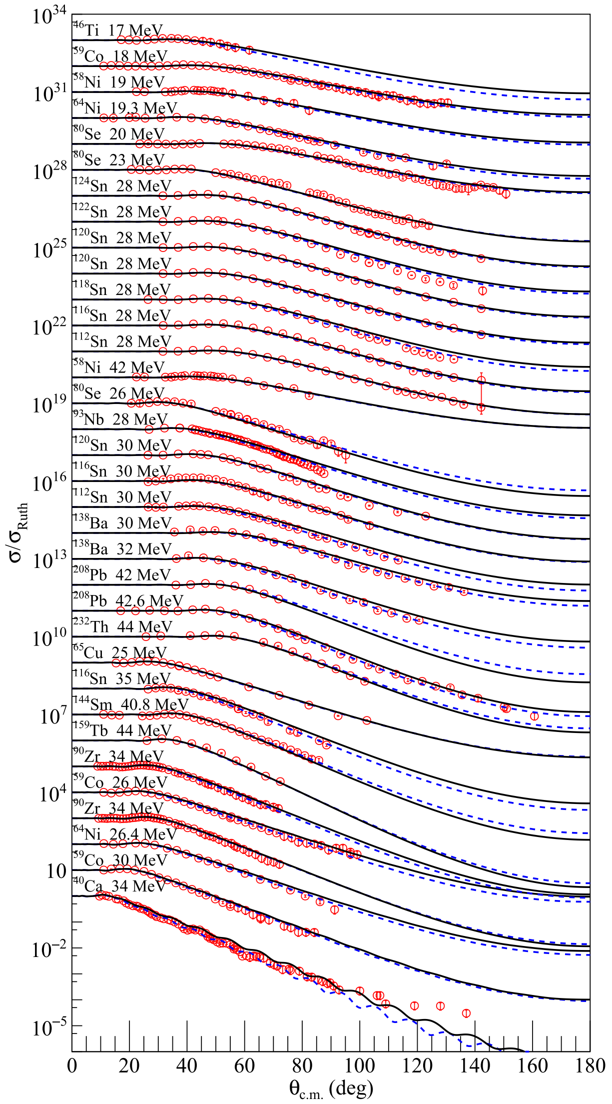

Fig. 4. (color online) Same as Fig. 1, but for ^{7}Li projectile. The experimental data are from Refs. [38–39, 44, 47, 52–53, 61−73].

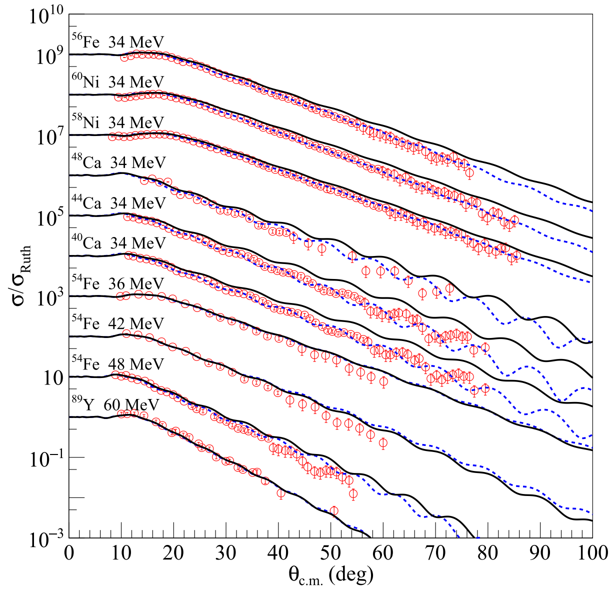

Fig. 5. (color online) Same as Fig. 1, but for ^{7}Li at higher energies. The experimental data are from Refs. [57, 66].

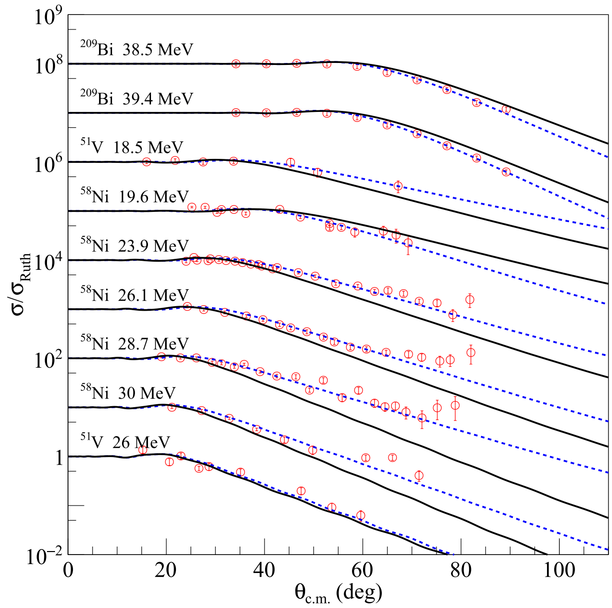

Fig. 6. (color online) Same as Fig. 1, but for ^{8}Li projectile. The experimental data are from Refs. [74−78].

clearly illustrated in Figs. 1, 2, and 3, for most of the ^{6}Li elastic scattering data, the angular distributions of the optimal fit exhibited a significant shift towards forward angles. This observation implies that, for ^{6}Li projectiles, larger rms proton radii than those obtained from Hartree-Fock calculations should be adopted in optical model calculations. A similar trend was also evident in the ^{7}Li elastic scattering results, although some angular distributions indicated shifts towards larger angles, as shown in Figs. 4 and 5. Conversely, the fitting results for most of the ^{8}Li data reveal that the differential cross sections calculated using the original density distributions need to be enhanced to better match the experimental data. However, this does not necessarily imply that the rms proton radius of ^{8}Li is lower than the Hartree-Fock prediction. First, the potential parameters used in the fitting procedure were derived from the elastic scattering data analysis of the stable nucleus ^{9}Be, and their applicability to ^{8}Li elastic scattering data remains uncertain. Second, as discussed in Ref. [75], the ^{8}Li + ^{58}Ni elastic scattering is significantly affected by coupled direct reaction channels. Coupled-reaction channels calculations, which consider the coupling between elastic scattering and neutron transfer channels populating bound and unbound states of ^{59}Ni, revealed that neutron stripping channels significantly affect elastic cross sections and particularly enhance cross sections at large angles. With respect to the results for the stable nuclei ^{10}B and ^{11}B shown in Fig. 7, discrepancies between the fitted angular distributions and calculations with unaltered density distributions were negligible, and both approaches could reasonably reproduce the experimental data. This result suggests that the rms proton radii of these two nuclei do not require significant modifications for use in optical model analysis of elastic scattering data. However, due to the limited availability of experimental data, additional investigations are necessary to extract more conclusive rms proton radii for ^{10}B and ^{11}B nuclei.

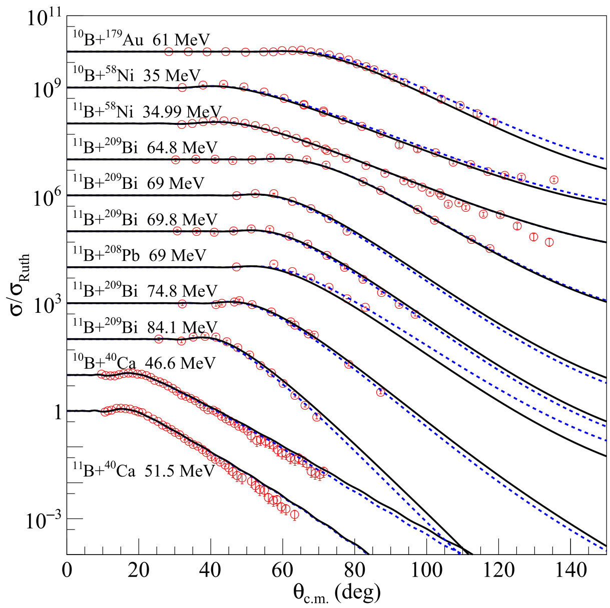

Fig. 7. (color online) Same as Fig. 1, but for ^{10}B and ^{11}B projectiles. The experimental data are from Refs. [79−84].

IV. EXTRACTION OF RMS PROTON RADII

Distributions of the rms proton radii values of ^{6,7,8}Li and ^{10,11}B extracted from individual elastic scattering data fittings are presented in Fig. 8.

In particular, the optimal rescaling factors for ^{6}Li and ^{7}Li predominantly cluster in the range of $\alpha > 1.00$. By contrast, the rescaling factors for ^{8}Li exhibit significant dispersion, and definitive conclusions remain a elusive challenge similarly encountered with ^{10}B and ^{11}B due to the limited number of data points. The average values of these distributions are adopted as the final rescaling factors for each projectile, demonstrating close correspondence to the central values of Gaussian functions fitted to the distributions. The final rescaling factors provide recommended rms proton radii for ^{6}Li, ^{7}Li, ^{8}Li, ^{10}B, and ^{11}B, corresponding to 2.35, 2.19, 1.94, 2.29, and 2.31 fm, respectively.

The extracted proton rms radii from elastic scattering data analysis for ^{6,7,8}Li and ^{10,11}B are shown in Fig. 9. The average rms proton radii (red filled circles) for ^{6}Li and ^{7}Li exceed the Hartree-Fock predictions (black filled squares), whereas an opposite trend is observed for ^{8}Li, consistent with the angular distribution results discussed earlier. Comparisons with experimental data derived from interaction cross sections [7], charge radii [2], and charge-changing cross sections [15] reveal that the extracted rms proton radii align more closely with experimental values than Hartree-Fock calculations, particularly for ^{10}B and ^{11}B. This underscores the effectiveness

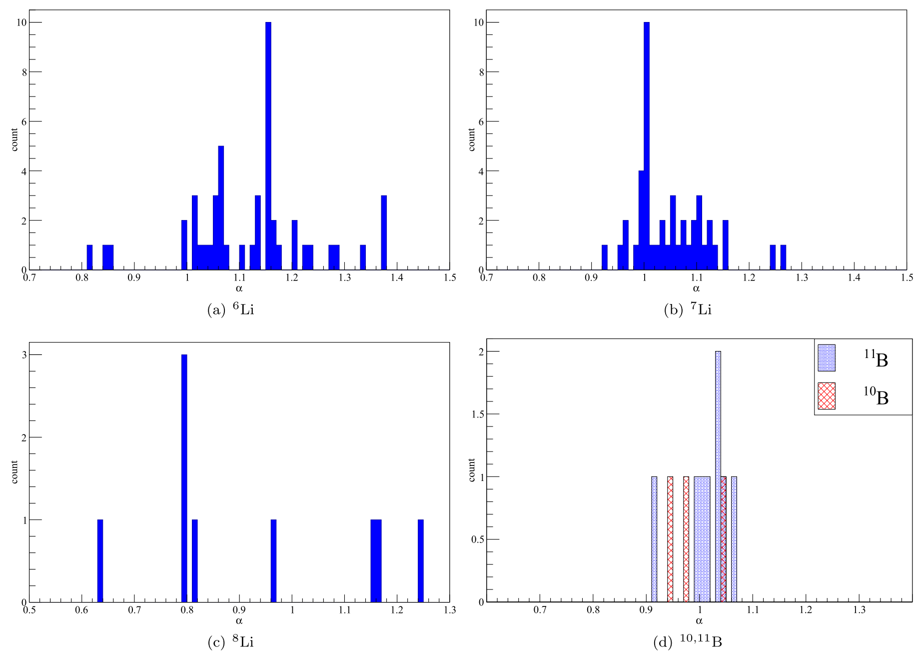

Fig. 8. (color online) Distributions of the rms proton radii values of ^{6,7,8}Li and ^{10,11}B.

Table 1. Experimental data analyzed in the present work for ^{6,7,8}Li, and ^{10,11}B from different targets, their references, and corresponding χ^2 values calculated with extracted rms proton radii.

Projectile	Target	Energy/MeV	Radii/fm	χ^2	Ref.
^{6}Li	^{40}Ca	240	2.55	11.72	[59]
	^{48}Ca	240	2.25	9.85	[59]
	^{58}Ni	20	2.18	1.96	[51]
	^{58}Ni	34	2.48	2.46	[43]
	^{58}Ni	73.7	2.88	22.39	[55]
	^{58}Ni	240	2.69	12.11	[60]
	^{59}Co	18	2.4	9.86	[47]
	^{59}Co	26	2.23	5.21	[47]
	^{59}Co	30	2.13	12.29	[47]
	^{64}Ni	19	2.15	3.22	[51]
	^{64}Ni	26	2.42	0.88	[51]
	^{64}Zn	19.98	2.88	31.66	[54]
	^{65}Cu	25	2.44	54.75	[53]
	^{70}Ge	28	2.46	1.03	[49]
	^{72}Ge	28	2.44	0.98	[49]
	^{74}Ge	28	2.42	0.74	[49]
	^{80}Se	23	2.42	1.00	[52]
	^{80}Se	26	2.21	1.03	[52]
	^{89}Y	60	2.59	0.92	[57]
	^{90}Zr	25	2.19	169.56	[48]
	^{90}Zr	30	2.23	62.23	[48]
	^{90}Zr	34	2.42	0.44	[44]
	^{90}Zr	60	2.21	2.84	[57]
	^{90}Zr	70	2.42	19.99	[56]
	^{90}Zr	73.7	2.46	8.73	[55]
	^{90}Zr	240	2.67	6.99	[60]
	^{91}Zr	34	2.42	0.84	[44]
	^{112}Sn	30	2.38	0.62	[45]
	^{112}Sn	30	2.57	7.82	[46]
	^{112}Sn	35	2.52	0.09	[42]
	^{116}Sn	30	2.31	0.06	[42]
	^{116}Sn	35	2.8	0.03	[42]
	^{116}Sn	240	2.88	5.21	[58]
	^{120}Sn	27	2.1	34.80	[50]
	^{120}Sn	44	1.73	11.11	[37]
	^{124}Sn	73.7	2.42	11.31	[55]
	^{144}Sm	32.2	2.23	2.82	[39]
	^{144}Sm	35.1	2.23	3.26	[39]
	^{144}Sm	42.3	2.23	9.50	[39]
	^{208}Pb	39	2.4	1.57	[41]

Continued on next page

Table 1-continued from previous page

Projectile	Target	Energy/MeV	Radii/fm	χ^2	Ref.
	^{208}Pb	43	1.79	9.65	[36]
	^{208}Pb	46	1.77	18.63	[36]
	^{208}Pb	73.7	2.42	2.26	[55]
	^{209}Bi	40	2.13	10.08	[35]
	^{209}Bi	40	2.13	10.03	[40]
	^{209}Bi	44	2.4	2.51	[35]
	^{209}Bi	50	2.21	42.61	[35]
	^{232}Th	44	2.08	0.48	[38]
^{7}Li	^{40}Ca	34	2.41	11.26	[65]
	^{40}Ca	34	2.59	9.23	[66]
	^{44}Ca	34	2.64	8.26	[66]
	^{46}Ti	17	2.34	3.09	[73]
	^{48}Ca	34	2.38	58.71	[66]
	^{54}Fe	36	2.09	5.14	[66]
	^{54}Fe	42	2.05	11.27	[66]
	^{54}Fe	48	2.3	10.11	[66]
	^{56}Fe	34	2.36	19.08	[66]
	^{58}Ni	19	2.15	5.25	[73]
	^{58}Ni	34	2.32	7.79	[66]
	^{58}Ni	42	2.07	0.90	[63]
	^{59}Co	18	2.15	2.81	[47]
	^{59}Co	26	2.3	2.01	[47]
	^{59}Co	30	2.2	8.01	[47]
	^{60}Ni	34	2.41	19.32	[66]
	^{64}Ni	19.3	2.2	0.23	[72]
	^{64}Ni	26.4	2.26	2.05	[72]
	^{65}Cu	25	2.09	27.99	[53]
	^{80}Se	20	2.09	3.03	[52]
	^{80}Se	23	2.07	2.37	[52]
	^{80}Se	26	1.99	1.99	[52]
	^{89}Y	60	2.09	1.50	[57]
	^{90}Zr	34	2.09	0.96	[66]
	^{90}Zr	34	2.24	0.47	[44]
	^{93}Nb	28	2.18	173.53	[71]
	^{112}Sn	28	2.07	130.56	[70]
	^{112}Sn	30	2.28	0.21	[68]
	^{116}Sn	28	2.09	893.60	[70]
	^{116}Sn	30	2.09	1.17	[64]
	^{116}Sn	35	2.3	0.94	[64]
	^{118}Sn	28	2.22	266.41	[70]
	^{120}Sn	28	2.09	92.42	[69]

Continued on next page

Table 1-continued from previous page

Projectile	Target	Energy/MeV	Radii/fm	χ^2	Ref.
	^{120}Sn	28	2.11	86.61	[70]
	^{120}Sn	30	2.09	226.13	[69]
	^{122}Sn	28	2.13	599.16	[70]
	^{124}Sn	28	2.09	184.44	[70]
	^{138}Ba	30	2.24	1.20	[67]
	^{138}Ba	32	2.28	0.89	[67]
	^{144}Sm	40.8	2.01	1.96	[39]
	^{159}Tb	44	2.07	9.17	[61]
	^{208}Pb	42	1.92	19.04	[62]
	^{208}Pb	42.6	2.2	0.92	[85]
	^{232}Th	44	2.01	7.38	[38]
^{8}Li	^{58}Ni	19.6	2.59	5.68	[74]
	^{58}Ni	23.9	1.69	2.40	[75]
	^{58}Ni	26.1	1.65	1.80	[75]
	^{58}Ni	27.8	1.32	2.93	[75]
	^{58}Ni	30	1.65	4.48	[75]
	^{51}V	18.5	1.65	0.35	[76]
	^{51}V	26	2.03	3.21	[77]
	^{209}Bi	38.5	2.42	0.82	[78]
	^{209}Bi	39.4	2.45	0.34	[78]
^{10}B	^{40}Ca	46.6	2.42	4.39	[79]
	^{58}Ni	35	2.26	10.14	[80]
	^{197}Au	61	2.19	10.49	[81]
^{11}B	^{40}Ca	51.5	2.33	9.40	[79]
	^{58}Ni	34.99	2.3	107.94	[84]
	^{208}Pb	69	2.1	184.11	[82]
	^{209}Bi	64.8	2.28	0.31	[83]
	^{209}Bi	69	2.37	7.66	[83]
	^{209}Bi	69.8	2.37	0.67	[83]
	^{209}Bi	74.8	2.4	1.51	[83]
	^{209}Bi	84.1	2.44	1.39	[83]

of optical model analysis based on USNP systematics for extracting nuclear rms proton radii from elastic scattering data.

V. SUMMARY

The optical model was employed to analyze the elastic scattering angular distributions of 112 datasets involving ^{6,7,8}Li and ^{10,11}B projectiles interacting with medium-mass and heavy targets at incident energies exceeding the Coulomb barriers. Subsequently, the rms proton radii of the projectiles were extracted. For the stable nuclei ^{6,7}Li and ^{10,11}B, the rms proton radii derived from the present analysis exhibited a more favorable agreement with experimental data than the predictions obtained from Hartree-Fock calculations. This outcome strongly suggests that the systematic analysis of elastic scattering data represents an effective approach for extracting nuclear rms proton radii. By contrast, the extracted rms proton radius of ^{8}Li was lower, which indicates the necessity of considering more intricate influences including the effects of strong couplings and the applicability of optical model parameters to weakly bound nuclei. Additionally, the current elastic scattering data for ^{8}Li are limited in

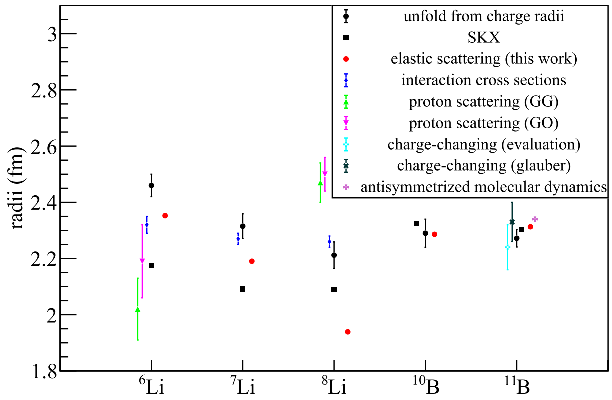

Fig. 9. (color online) Comparison of this work with other experimental and theoretical rms proton radii. References are listed as follows: unfold from charge radii [2]. interaction cross sections [7]. charge-changing(Glauber) [15]. charge-changing(evaluation) [15]. anti-symmetrized molecular dynamic [15]. isotope shift [86]. proton scattering(GG) [86]. proton scattering(GO) [86]. Skyrme Hartree-Fock [20].

terms of the incident energy range and variety of target nuclei investigated. Consequently, further experimental studies on ^{8}Li are necessary to enable the extraction of rms proton radii using a systematic methodology.

References

[1] T. Li, Y. Luo, and N. Wang, Atomic Data and Nuclear Data Tables **140**, 101440 (2021)
[2] I. Angeli and K. Marinova, Atomic Data and Nuclear Data Tables **99**, 69 (2013)
[3] R. Hofstadter, H. R. Fechter, and J. A. McIntyre, Phys. Rev. **92**, 978 (1953)
[4] T. E. Cocolios (2020).
[5] Z.-T. Lu, P. Mueller, G. W. F. Drake *et al.*, Rev. Mod. Phys. **85**, 1383 (2013)
[6] I. Tanihata, H. Hamagaki, O. Hashimoto *et al.*, Phys. Lett. B **160**, 380 (1985)
[7] I. Tanihata, H. Hamagaki, O. Hashimoto *et al.*, Phys. Rev. Lett. **55**, 2676 (1985)
[8] I. Tanihata, T. Kobayashi, O. Yamakawa *et al.*, Phys. Lett. B **206**, 592 (1988)
[9] A. Ozawa, I. Tanihata, T. Kobayashi *et al.*, Nucl. Phys. A **608**, 63 (1996)
[10] Y. Ogawa, K. Yabana, and Y. Suzuki, Nucl. Phys. A **543**, 722 (1992)
[11] J. S. Al-Khalili and J. A. Tostevin, Phys. Rev. Lett. **76**, 3903 (1996)
[12] T. Yamaguchi, I. Hachiuma, A. Kitagawa *et al.*, Phys. Rev. Lett. **107**, 032502 (2011)
[13] A. Estradé, R. Kanungo, W. Horiuchi *et al.*, Phys. Rev. Lett. **113**, 132501 (2014)
[14] G. Satchler and W. Love, Phys. Rep. **55**, 183 (1979)
[15] Y. Kanada-En'yo, Phys. Rev. C **91**, 014315 (2015)
[16] Y. Kanada-En'yo, M. Kimura, and H. Horiuchi, Comptes Rendus Physique **4**, 497 (2003)
[17] R. A. Mohammed and W. Z. Majeed , Phys. Atom. Nucl. **86**, 77 (2023)
[18] E. Tel, S. Okuducu, G. Tanir *et al.*, Communications in Theoretical Physics **49**, 696 (2008)
[19] F. Tondeur, Phys. Lett. B **123**, 139 (1983)
[20] B. Alex Brown, Phys. Rev. C **58**, 220 (1998)
[21] G. Yang, D. Y. Pang, Y. Y. Yang *et al.*, Phys. Rev. C **107**, 044603 (2023)
[22] D. Y. Pang, Y. L. Ye, and F. R. Xu, Phys. Rev. C **83**, 064619 (2011)
[23] Y. P. Xu and D. Y. Pang, Phys. Rev. C **87**, 044605 (2013)
[24] X. F. Zhang and D. Y. Pang, Chin. Phys. Lett. **31**, 052401 (2014)
[25] F. A. Bumiller, F. R. Buskirk, J. N. Dyer *et al.*, Phys. Rev. C **5**, 391 (1972)
[26] T. Stovall, J. Goldemberg, and D. Isabelle, Nucl. Phys. **86**, 225 (1966)
[27] F. Kondev, M. Wang, W. Huang *et al.*, Chin. Phys. C **45**, 030001 (2021)
[28] W. Nörtershäuser, T. Neff, R. Sánchez *et al.*, Phys. Rev. C **84**, 024307 (2011)
[29] B. Maaß, T. Hüther, K. König *et al.*, Phys. Rev. Lett. **122**, 182501 (2019)
[30] B. Brown, W. Richter, and R. Lindsay, Phys. Lett. B **483**, 49 (2000)
[31] B. A. Brown, S. Typel, and W. A. Richter, Phys. Rev. C **65**, 014612 (2001)
[32] J. Lee, J. A. Tostevin, B. A. Brown *et al.*, Phys. Rev. C **73**, 044608 (2006)
[33] W. A. Richter and B. A. Brown, Phys. Rev. C **67**, 034317 (2003)
[34] IAEA. Experimental nuclear reaction data (2025) https://www-nds.iaea.org/exfor/
[35] S. Santra, S. Kailas, K. Ramachandran *et al.*, Phys. Rev. C **83**, 034616 (2011)
[36] C.-L. Zhang, H.-Q. Zhang, C.-J. Lin *et al.*, Chin. Phys. Lett. **23**, 1146 (2006)
[37] K. Becker, K. Blatt, H. Jnsch *et al.*, Nucl. Phys. A **535**, 189 (1991)
[38] S. Dubey, S. Mukherjee, D. C. Biswas *et al.*, Phys. Rev. C **89**, 014610 (2014)
[39] J. M. Figueira, J. O. F. Niello, A. Arazi *et al.*, Phys. Rev. C **81**, 024613 (2010)
[40] S. Santra, V. Parkar, K. Ramachandran *et al.*, Phys. Lett. B

677, 139 (2009)
[41] N. Keeley, S. Bennett, N. Clarke *et al*., Nucl. Phys. A **571**, 326 (1994)
[42] N. N. Deshmukh, S. Mukherjee, D. Patel *et al*., Phys. Rev. C **83**, 024607 (2011)
[43] K. D. Veal, C. R. Brune, W. H. Geist *et al*., Phys. Rev. C **60**, 064003 (1999)
[44] R. Puigh and K. Kemper, Nucl. Phys. A **313**, 363 (1979)
[45] D. Chattopadhyay, S. Santra, A. Pal *et al*., Phys. Rev. C **94**, 061602 (2016)
[46] D. Chattopadhyay, S. Santra, A. Pal *et al*., Phys. Rev. C **102**, 021601 (2020)
[47] F. A. Souza, L. A. S. Leal, N. Carlin *et al*., Phys. Rev. C **75**, 044601 (2007)
[48] H. Kumawat, V. Jha, B. J. Roy *et al*., Phys. Rev. C **78**, 044617 (2008)
[49] M. D. L. Barbosa, T. Borello-Lewin, L. B. HorodynskiMatsushigue *et al*., Phys. Rev. C **71**, 024303 (2005)
[50] V. A. B. Zagatto, M. Gómez-Ramos, L. R. Gasques *et al*., Phys. Rev. C **106**, 014622 (2022)
[51] M. Biswas, S. Roy, M. Sinha *et al*., Nuclear Physics A **802**, 67 (2008)
[52] L. Fimiani, J. M. Figueira, G. V. Martí *et al*., Phys. Rev. C **86**, 044607 (2012)
[53] A. Shrivastava, A. Navin, N. Keeley *et al*., Physics Letters B **633**, 463 (2006)
[54] M. Zadro, P. Figuera, A. D. Pietro *et al*., Phys. Rev. C **80**, 064610 (2009)
[55] R. Huffman, A. Galonsky, R. Markham *et al*., Phys. Rev. C **22**, 1522 (1980)
[56] D. J. Horen, R. L. Auble, J. Gomez del Campo *et al*., Phys. Rev. C **47**, 629 (1993)
[57] R. Wadsworth, M. D. Cohler, M. J. Smithson *et al*., J. Phys. G: Nucl. Phys. **9**, 1237 (1983)
[58] X. Chen, Y.-W. Lui, H. L. Clark *et al*., Phys. Rev. C **76**, 054606 (2007)
[59] Krishichayan, X. Chen, Y.-W. Lui *et al*., Phys. Rev. C **81**, 044612 (2010)
[60] Krishichayan, X. Chen, Y. W. Lui *et al*., Phys. Rev. C **81**, 014603 (2010)
[61] D. Patel, S. Mukherjee, D. C. Biswas *et al*., Phys. Rev. C **91**, 054614 (2015)
[62] D. Gupta, C. Samanta, A. Chatterjee *et al*., Nucl. Phys. A **683**, 3 (2001)
[63] D. Gupta, C. Samanta, R. Kanungo *et al*., Nucl. Phys. A **646**, 161 (1999)
[64] N. N. Deshmukh, S. Mukherjee, B. K. Nayak *et al*., Eur. Phys. J. A **47**, 118 (2011)
[65] D. P. Sanderson, S. P. Van Verst, J. Cook *et al*., Phys. Rev. C **32**, 887 (1985)
[66] C. Glover, R. Cutler, K. Kemper, Nucl. Phys. A **341**, 137 (1980)
[67] A. M. M. Maciel, P. R. S. Gomes, J. Lubian *et al*., Phys. Rev. C **59**, 2103 (1999)
[68] D. Chattopadhyay, S. Santra, A. Pal *et al*., Phys. Rev. C **98**, 014609 (2018)
[69] A. Kundu, S. Santra, A. Pal *et al*., Phys. Rev. C **95**, 034615 (2017)
[70] A. Kundu, S. Santra, A. Pal *et al*., Phys. Rev. C **99**, 034609 (2019)
[71] S. K. Pandit, A. Shrivastava, K. Mahata *et al*., Phys. Rev. C **93**, 061602 (2016)
[72] M. M. Shaikh, M. Das, S. Roy *et al*., Nucl. Phys. A **953**, 80 (2016)
[73] T. P. Morrison, G. D. Jones, L. P. Ekstrom *et al*., J. Phys. G: Nucl. Phys. **5**, 1751 (1979)
[74] F. D. Becchetti, W. Z. Liu, K. Ashktorab *et al*., Phys. Rev. C **48**, 308 (1993)
[75] O. C. B. Santos, R. Lichtenthäler, K. C. C. Pires *et al*., Phys. Rev. C **103**, 064601 (2021)
[76] S. Mukherjee, N. N. Deshmukh, V. Guimarães *et al*., Eur. Phys. J. A **45**, 23 (2010)
[77] A. Lépine-Szily and R. Lichtenthler, Nucl. Phys. A **787**, 94 (2007)
[78] K. J. Cook, I. P. Carter, E. C. Simpson *et al*., Phys. Rev. C **97**, 021601 (2018)
[79] C. Glover, K. Kemper, L. Parks *et al*., Nucl. Phys. A **337**, 520 (1980)
[80] V. Scarduelli, E. Crema, V. Guimarães *et al*., Phys. Rev. C **96**, 054610 (2017)
[81] L. R. Gasques, L. C. Chamon, A. Lépine-Szily *et al*., Phys. Rev. C **101**, 044604 (2020)
[82] P. K. Sahu, A. Saxena, R. K. Choudhury *et al*., Phys. Rev. C **68**, 054612 (2003)
[83] A. Shrivastava, S. Kailas, P. Singh *et al*., Nucl. Phys. A **635**, 411 (1998)
[84] N. N. Deshmukh, V. Guimarães, E. Crema *et al*., Phys. Rev. C **92**, 054615 (2015)
[85] L. Yang, C. J. Lin, H. M. Jia *et al*., Phys. Rev. C **89**, 044615 (2014)
[86] H. Sakaguchi and J. Zenihiro, Prog. Part. Nucl. Phys. **97**, 1 (2017)